Soft Matter

Cite this: *Soft Matter*, 2012, **8**, 2860

www.rsc.org/softmatter

**PAPER**

# Phase equilibrium and structure formation in gold nanoparticles—nematic liquid crystal composites: experiments and theory†

**Ezequiel R. Soulé,[ab] Jonathan Milette,[c] Linda Reven[c] and Alejandro D. Rey*[b]**

***Received 2nd November 2011, Accepted 23rd December 2011***
**DOI: 10.1039/c2sm07091j**



A theoretical and experimental study of mixtures of a calamitic nematic liquid crystal and gold nanoparticles capped with mixed monolayers (alkylic + mesogenic ligands) is presented. The effect of the ligand monolayer composition and nanoparticle concentration on the solubility in the isotropic phase and on the isotropic–nematic phase transition is studied. Mixed monolayers show the highest miscibility and lead to the formation of well-defined cellular networks. This behaviour is explained in terms of a mean-field thermodynamic model, in combination with a phenomenological expression for the isotropic interaction parameter that accounts for entropic and enthalpic effects of the mixed ligand monolayer. The final structure of the material is shown to be determined essentially by the phase equilibrium behaviour.

## 1. Introduction

Liquid crystals (LC) have attracted attention over the years as electro-optic materials with applications in display technology, sensors, light valves, switchable windows, and others.[1–4] More recently, they have been used as dispersing medium for colloidal particles and nanoparticles (NPs) as a flexible method for generating and controlling self-assembly into complex structures.[5–10] Micron and sub-micron particles create local distortions in the director orientation field, which give rise to short and long range interactions[10,11] due to the elastic energy associated with the distortions. This effect can result in phase separation and the formation of different structures, like cellular networks[5–8] and linear or two-dimensional arrays of particles;[11–13] these structures can have a significant effect on material properties. For "large" particles (compared to molecular size), the elastic energy dominates the free energy and dictates the phase behaviour.[11,13] As the size of the particles decrease and they become comparable in size to the LC molecules, they behave as a molecular component and entropic effects must be taken into account to properly describe the phase behaviour of the system. The mixing entropy and entropy-driven self-assembly (hard-sphere crystallization) are expected to be relevant.

Controlling the dispersion and self-assembly of the NPs in the host matrix is crucial for most applications.[14–16] Surface functionalization of the NP can provide the means to stabilize the dispersion when the right combination ligand–solvent is used.[16–18] Grafting a ligand layer on the NPs surface provides a steric repulsion that can be enough to overcome van der Waals attractions, but it also modifies the interactions between the particle and the solvent. This effect can be very important for the case of NPs and has to be taken into account.

In this work, we use a thermodynamic solution model for describing phase equilibrium in NP–LC mixtures[19,20] to analyze experimentally observed phase-separated structures in a mixture of gold NPs and a nematic LC. The NPs are capped with a monolayer composed of a mixture of two different ligands. We introduce a phenomenological expression for the mixing interaction parameter that accounts for entropic and enthalpic effects due to the interaction of the LC host and the mixed ligands in the NP corona. The extent of particle aggregation and the formation of network structures under different experimental conditions can be qualitatively described by this model.

The organization of this paper is as follows. Section 2 describes the experimental techniques used. In Section 3 we introduce the thermodynamic model. Experimental results and theoretical predictions are presented in Section 4. The phenomenological model for the mixing interaction parameter is introduced and results based on this model are presented. Finally, Section 5 presents the conclusions.

## 2. Experimental

### Materials

4-Cyano-4′-*n*-pentylbiphenyl (5CB) was purchased from Synthon Chemicals and used as received.

[a]*Institute of Materials Science and Technology (INTEMA), University of Mar del Plata and National Research Council (CONICET), J. B. Justo 4302, 7600 Mar del Plata, Argentina. E-mail: ersoule@fi.mdp.edu.ar*
[b]*Department of Chemical Engineering, McGill University, 3610 University st, Montreal, Quebec, H3A2B2, Canada*
[c]*Center for Self-Assembled Chemical Structure (CSACS), Chemistry Department, McGill University, 801 Sherbrooke St West, Montreal, Quebec, H3A 2K6, Canada*

† Electronic supplementary information (ESI) available: POM images of network formation. See DOI: 10.1039/c2sm07091j

The synthesis of the monolayer and mixed monolayer of 4.5 nm diameter gold nanoparticles (NPs) *via* exchange reactions with 4-(*N*,*N*-dimethylamino)pyridine (DMAP)-stabilized NPs is reported in an earlier publication.[21] Mixtures of two different types of ligands, hexanethiol and 4′-(12-mercaptododecyloxy) biphenyl-4-carbonitrile, were used. The total number of ligands per particle varied between 218 and 270. The different compositions of the ligand shell, expressed as the percentage of area covered by the mesogenic ligand, were: 0, 28, 49, 70 and 100. In what follows, we will refer to each nanoparticle as NP-*X*, where *X* is the area coverage of the mesogenic ligand.

### Sample preparation

The LC was mixed with the GNPs using dichloromethane, the solution was sonicated for 1 min and the solvent evaporated under a stream of Ar(g) (overnight) and vacuum (1 h). Some samples were subjected to overnight vacuum drying with heating to the isotropic phase to eliminate the possibility of residual solvent acting as a third component but these samples showed the same behaviour. Prior to the preparation of the optical microscopy slides, the dispersion was sonicated above the nematic–isotropic phase transition and manually stirred at room temperature with the pipette used to transfer the material, which is in the nematic phase, to the glass slide. Another glass slide was put on top of the first one, and the dry sample was sandwiched between the two glass slides.

### Transmission optical microscopy

The dispersions were heated to the isotropic phase and mixed by moving and pressing the two slides together. Polarized optical microscopes (Zeiss or Canon) with parallel and cross-analyzers were used and mounted with a Mettler FP900 heating stage or Instec processor/Mettler FP82 hot stage. A cooling rate of 1 °C $min^{-1}$ was used.

## 3. Model

The model used in this work is based on a thermodynamic theory proposed by Matsuyama and Hirashima,[19] with some modifications, as presented elsewhere.[20] We consider the system as composed of a mixture of calamitic nematic LC and hard spherical NPs. The two species are characterized by their specific volume, $v$, and area per unit volume, $a$. In the case of the LC, $v_{LC} = \pi R_{LC}^2 L_{LC}$, $a_{LC} = 2/R_{LC} + 2/L_{LC}$, and for the NP, $v_{NP} = 4/3\pi R_{NP}^3$, $a_{NP} = 3/R_{NP}$, where $R_{LC}$ and $L_{LC}$ are the radius and length of a LC molecule and $R_{NP}$ the radius of a nanoparticle. The lengths and volumes are non-dimensionalized by scaling with respect to a reference length, $l_R$, and a reference volume, $l_R^3$. The number of LC molecules and NPs in the mixture are $N_{LC}$ and $N_{NP}$, and the total volume is $V$. The dimensionless free energy of the mixture is:

$$f = \frac{l^3 F}{V R_g T} = f_{iso} + f_{nem} + f_{crys} + f_{int} \quad (1)$$

where $F$ is the total free energy, $R_g$ is the universal gas constant and $T$ the absolute temperature, and four contributions are considered: isotropic mixing free energy ($f_{iso}$), nematic ordering ($f_{nem}$), crystalline ordering ($f_{crys}$) and specific interactions ($f_{int}$). The isotropic mixing free energy can be approximated by:

$$f_{iso} = \frac{\phi_{LC}}{v_{LC}} \ln(\phi_{LC}) + \frac{\phi_{NP}}{v_{NP}} \ln(\phi_{NP}) + \frac{\phi_{NP}}{v_{NP}} \frac{(4\phi_{NP} - 3\phi_{NP}^2)}{(1-\phi_{NP})^2} + \chi a_p \phi_{NP} \varphi_{LC} \quad (2)$$

where $\phi_i = N_i v_i / V$, for i = LC, NP, are the volume fractions of each species ($\phi_{NP} + \phi_{LC} = 1$). The first two terms are the Flory Huggins mixing entropy and the third term is calculated from Carnahan–Starling equation of state for hard spheres,[22–24] and accounts for excluded-volume effects between particles. The last term accounts for isotropic binary interactions and takes into account that the interactions are proportional to the area of contact between LC molecules and NPs, the factor $\phi_{NP} a_{NP}$ is proportional to the total area of NPs and $\varphi_{LC} = \phi_{LC} a_{LC} / (\phi_{LC} a_{LC} + \phi_{NP} a_{NP})$ is the area fraction of liquid crystal and represents the probability that the NP surface is in direct contact with a LC.[24] $\chi = A + B/T$ is the isotropic binary interaction parameter.

The nematic free energy is calculated from the Maier–Saupe theory:[25,26]

$$f_{nem} = \frac{\phi_{LC}}{v_{LC}} \left[ \frac{1}{2} \nu \varphi_{LC} S^2 - \ln(Z_n) \right] \quad (3)$$

where $S$ is the scalar nematic order parameter, $Z_n$ the nematic partition function and $\nu$ is the Maier–Saupe quadrupolar interaction parameter. Once again the area fraction is used as the probability of contact. The logarithm of the partition function is approximated by a sixth-order polynomial expression, which is much more efficient from a computational point of view.[27]

The crystalline free energy is written according to the mean-field model presented by Matsuyama and Hirashima,[19] and it is analogous to the nematic free energy;

$$f_{cris} = \frac{\phi_{NP}}{v_{NP}} \left[ \frac{1}{2} g \phi_P \sigma^2 - \ln Z_c \right] \quad (4)$$

where $\sigma$ is the crystal order parameter, $Z_c$ is the crystal partition function and $g$ is an excluded-volume interaction parameter, which for hard spheres is 14.95.[19] As in the nematic case, the crystal partition function was approximated with a polynomial obtained from a least-squares fitting.

Finally, the last contribution to the free energy is due to specific interactions, following Matsuyama we write this term as:

$$f_{int} = w S^2 a_P \phi_P \varphi_{LC} \quad (5)$$

where $w$ is a binary nematic interaction that accounts for anchoring at the NP surface and distortions in the nematic director at a nanoscale in the vicinity of a NP. We consider these interactions to be proportional to the area of contact and we neglect the coupling interactions between nematic and crystalline ordering.

The construction of this phase diagram follows standard procedures: the equilibrium condition at each temperature is given by the equality of chemical potentials of each component and the minimization of the free energy with respect to the order parameter, in each phase. The isotropic–isotropic (I–I) critical point can be calculated as the point at which the second and third

derivatives of the isotropic free energy with respect to the composition are equal to 0:

$$\frac{1}{v_{LC}\phi_{LC}}+\frac{1}{v_{NP}\phi_{NP}}+\frac{2(4-\phi_{NP})}{v_{NP}(1-\phi_{NP})^4}-2\chi\frac{a_{LC}{}^2a_{NP}{}^2}{[a_{LC}\phi_{LC}+a_{NP}\phi_{NP}]^3}=0 \quad (6)$$

$$\frac{1}{v_{LC}\phi_{LC}{}^2}-\frac{1}{v_{NP}\phi_{NP}{}^2}+\frac{6(5-\phi_{NP})}{v_{NP}(1-\phi_{NP})^5}+6\chi\frac{a_{LC}{}^2a_{NP}{}^2(a_{NP}-a_{LC})}{[a_{LC}\phi_{LC}+a_{NP}\phi_{NP}]^4}=0 \quad (7)$$

For each temperature, the equilibrium condition is described by a system of algebraic equations, which are solved with a Newton–Rapson algorithm.

As mentioned before, in this work the NPs are treated as spheres and the LC molecules as cylinders. As the particles consist of a gold core and a ligand shell, the total volume of the particle is calculated by adding the volume of the core and the volume occupied by the ligands. The molar volume of the ligands and the solvent is calculated as $M/\rho$, where $M$ is the molar mass and $\rho$ the density (taken as 1 g cm$^{-3}$). The effective radius of the NP is calculated as $R_{NP} = (v_{NP} \times 3/(4\pi))^{1/3}$, and this is used to calculate $a_p = 4\pi R_{NP}{}^2/v_{NP}$. The volume of the gold core is calculated assuming that the core is a sphere of diameter 4.5 nm. The aspect ratio ($L_{LC}/2R_{LC}$) of the liquid crystal 5CB is taken as 3.5. A total number of ligands of 240 was taken, independently of the ligand shell composition. The reference length was taken as the effective diameter of 5CB, $l_R = 0.53$ nm.

## 4. Results and discussion

The general phase behaviour predicted by the thermodynamic theory was discussed in previous works.[19,20] Four different phases can be distinguished based in this mean-field model: isotropic (I) characterized by $S = 0$ and $\sigma = 0$; nematic (N), where $S > 0$ and $\sigma = 0$, crystal (C), where $S = 0$ and $\sigma > 0$, and nematic-crystal (NC), where $S > 0$ and $\sigma > 0$. Phase stability and phase coexistence regions for different values of the interaction parameters and particles radius were calculated in those works.

An experimental study of miscibility and structure formation during the phase separation, analyzing the effect of the experimental conditions on the final morphology was presented elsewhere.[21,28] Another study of a similar system but with smaller nanoparticles was also performed by Qi and Hegmann.[29,30] We will present here a summary of experimental results regarding miscibility and morphologies, obtained from these previous works and from new experiments. Tables 1 and 2 summarize qualitatively the observed phase behaviour of different mixtures; Table 1 corresponds to dispersions of the mixed ligand NP-$X$ in 5CB, where $X$ corresponds to the fraction of mesogenic ligands, and the NP concentration of the dispersions is 1 wt% gold. Table 2 presents the results of dispersions of NP-49 with different concentrations of NPs.

Different types of structures are identified in Tables 1 and 2. Network structures refer to cellular networks where distinct nematic domains can be identified, separated by clearly identifiable boundaries (see ESI†, Fig. S1 and S2, and ref. 28). Two types of domain boundaries are observed: low contrast boundaries (the cases identified as "weak network"), and high contrast, dark boundaries ("well defined network"). In this network, the nematic liquid crystal is homeotropic with respect to the glass surface when the thickness of the sample is small, and it shows Schlieren textures for thicker samples (a possible explanation for this is that the nanoparticles migrate to the glass surface and induce a homeotropic anchoring).[28–30] The cases identified in the tables as "Schlieren" (homogeneous or with aggregates), refer to cases where the Schlieren texture is continuous and do not show domain walls.[28]

**Table 1** Summary of experimental observations for NP dispersions in 5CB with 1 wt% gold (approx. 0.5%volume), based on POM observations

| Type of NP | Solubility above $T_{NI}$ | Phase separation below $T_{NI}$ | Final structure (cooling 1 °C min$^{-1}$) |
|---|---|---|---|
| NP-0 | Very low | No | Schlieren *w*/aggregates |
| NP-28 | Partial | Yes | Weak network |
| NP-49 | Total | Yes | Well defined network |
| NP-70 | Partial | Yes | Weak network |
| NP-100 | Partial | Yes | Weak network |

**Table 2** Summary of experimental observations for different dispersions of NP-49 in 5CB, based on POM observations. The calculated NP vol% includes both the volume of the gold core and the ligands

| Gold wt%/ NP vol% | Solubility above $T_{NI}$ | Phase separation below $T_{NI}$ | Final structure (cooling 1 °C min$^{-1}$) |
|---|---|---|---|
| 0.1/0.04 | Total | No | Homogeneous Schlieren |
| 0.5/0.21 | Total | No | Homogeneous Schlieren |
| 1/0.42 | Total | Yes | Well defined network |
| 5/2.14 | Total | Yes | Well defined network |
| 15/6.83 | Partial | Yes | Well defined network (strongest definition) |

An important observation from Table 1 is that the solubility of the nanoparticles in the isotropic phase depends strongly on the ligand shell composition.[21,28–30] The miscibility is highest for NP capped with a mixed monolayer, and lowest for particles with no mesogenic ligands. Table 2 shows that even for the most soluble particles (NP-49) miscibility is not complete; the maximum amount of NPs that can be dissolved is between 5 and 15 wt%. The second observation is that phase separation below $T_{NI}$ leads to a network structure, which is best defined (in terms of optical contrast) for NP-49 at high NP concentrations (this network structure was not observed for smaller NPs[29,30]).

Phase separation below $T_{NI}$ requires at least partial solubility in the isotropic phase, and a concentration of NP higher or equal to 1 wt%.[28] If there is some degree of solubility of the NPs in the nematic phase, at very low concentrations the NPs might remain completely dissolved in the nematic phase, and the phase transition process and the final morphology are not significantly different from those of the pure liquid crystal.

The process of formation of a cellular network is similar to other systems and it is as follows (micrographs of this process for two mixtures are presented in the ESI†, Fig. S1 and S2, see also ref. 28): as the temperature is decreased below $T_{NI}$, dispersed droplets of a nematic phase nucleate, grow and start to coalesce when they come into contact. As the growth–coalescence process evolves, essentially all the droplets come into contact, the



 

isotropic phase is confined in the intermediate spaces, and the network structure emerges. The arms, or branches, of the network are the boundaries between the nematic domains. As mentioned before, two different types of boundaries can be identified: higher contrast boundaries (see Fig. S1†), which are assumed to be the remaining isotropic phase, and lower contrast boundaries (Fig. S2†), which are ascribed to some type of defect walls between nematic domains, with a higher NP concentration than the bulk nematic phase, and lower than the bulk isotropic phase (analysing the exact nature and structure of these domain walls is beyond the scope of the present work). Materials with a prevalence of higher contrast boundaries are identified as a "well defined network", while low contrast boundaries correspond to a "weak network". According to this description, a material with a relatively high amount of isotropic phase will have a prevalence of high-contrast boundaries and its structure will be a "well defined network". In materials where most of the isotropic phase is converted to nematic, domain boundaries consist in nematic defects and the material shows a "weak network". Stronger network definitions are then directly related with the amount of remaining isotropic phase. In addition, the network density is different, it can be observed in Fig. S1 and S2† and in ref. 28 that the nucleation process is strongly affected by the nature of the ligands and the NP concentration, and this determines the final density of the network structure.

Comparing the cases of weak and well defined networks in Tables 1 and 2, it is observed that a higher solubility (for a given concentration), and a higher concentration (for a given ligand composition), of NPs, increase the amount of isotropic phase in the final structure. In the case of 1% NP-49, it was observed that some branches are formed by the isotropic phase and some by defect walls; in addition, for thin films part of the isotropic phase forms spherical nodes at the intersections of the branches.[28] In the case of 15% NP-49, essentially all the branches are formed by isotropic phase and the network is the most defined in terms of contrast.

As mentioned below, one of the factors determining the final structure is the initial solubility in the isotropic phase.[21,28] The change in miscibility can be ascribed to several factors. The simplest is the change in the particle geometric parameters, $v_{NP}$ and $a_{NP}$ (the nanoparticle is considered to be the totality of the gold core and the ligand shell), that affect the mixing free energy as can be seen in the model equations, but this effect alone cannot account for the differences observed between the different particles. In addition to this factor, the fact that the particles are not hard solid spheres as assumed in the model has to be considered: they have a soft shell that can be partially penetrated by the solvent (this is schematically shown in Fig. 1). This has an energetic effect and also an entropic effect. The energetic effect arises because the solvent is in contact with this ligand shell, so the enthalpy of the system will be a function of the ligand shell composition (an illustration of the interaction between solvent and the different groups in the ligand shell is shown by solid grey arrows in Fig. 1). The entropic effect is related to penetration of the solvent in the ligand shell. As can be seen in Fig. 1, there is some free volume in the outer layer of the ligand shell, so the LC solvent can partially "mix" with the mesogenic groups of the ligands (it is assumed that the inner alkylic layer is compact and impenetrable).

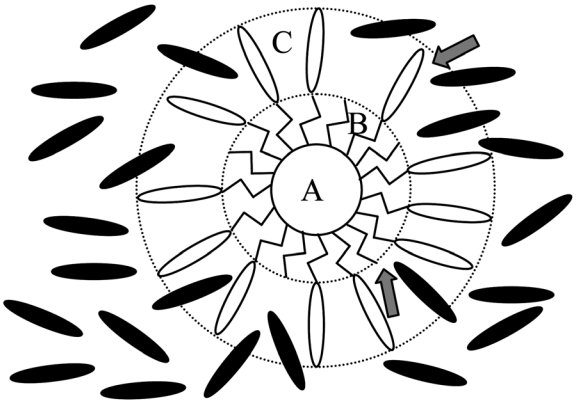


**Fig. 1** Schematic of a particle coated with a mixed ligand layer, in the presence of LC solvent (black ellipsoids). Region A is the gold core, Region B is the inner layer composed of alkyl chains (zigzag lines), and Region C is the outer layer composed of the mesogenic group of the ligands (white ellipsoids). Examples of LC solvent molecules in direct contact with an alkanethiol chain and with a liquid-crystalline ligand are indicated by the grey arrows.

A complete molecular model should take into account this effect with a detailed expression of the entropy and enthalpy due to the presence of this "soft corona" of ligands.[24] As a first approximation, these effects can be phenomenologically taken into account in a simple way by a suitable dependence of the binary isotropic interaction parameter on the ligand shell composition. The energetic part of the interaction parameter should be written as a linear function of the number of contacts between solvent–alkanethiol ligand and solvent–liquid crystalline ligands. The entropic part of the interaction parameter should take into account the free-volume effect, this effect is expected to be minimum in the extremes of non-mesogenic ligand and 100% mesogenic ligands, because in both cases the interpenetration is minimal. Taking into account this description, we can consider the energetic part of the interaction parameter to be a linear function of the concentration of ligands, and the entropic part of the interaction parameter to be a parabolic function with a minimum for intermediate compositions. We write $B = B_1\theta + B_2(1 - \theta)$, where $\theta$ is the fraction of the surface covered

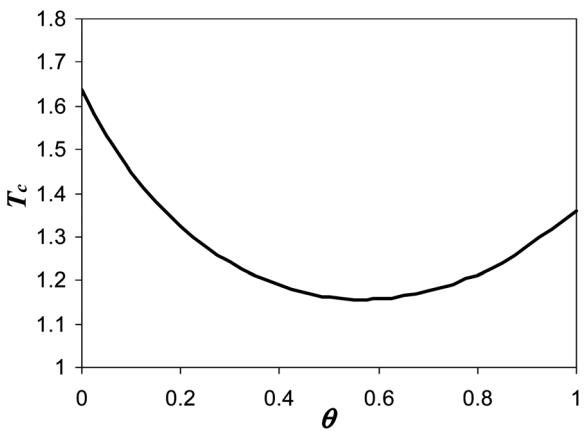


**Fig. 2** I–I critical temperature as a function of the content of mesogenic ligands in the NP ligand shell.

by mesogenic ligands, $B_1$ is the value for a pure mesogenic shell, and $B_2$ is the value for a pure alkylic shell (considering the chemical similarity, the restriction $B_2 > B_1$ should hold); and $A = A_0[(\theta - 0.5)^2 - 0.25]$ (this is a symmetric parabola which is 0 at the extremes and has the minimum at $\theta = 0.5$).

Fig. 2 shows the calculated I–I critical temperature for values of $A_0 = 2.8$, $B_1 = 3.8$, and $B_2 = 3.5$. These values were chosen to qualitatively represent the experimentally observed behaviour. The predicted critical temperature has a minimum for an intermediate value of $\theta$ and for $\theta = 0$ it is higher than that for $\theta = 1$. This means that the maximum solubility exists for some intermediate $\theta$, and that the miscibility is higher for pure mesogenic ligands compared to pure alkylic ligands, as observed experimentally.[21]

Fig. 3 shows calculated phase diagrams for three cases: low miscibility ($\theta = 0$, Fig. 3a), high miscibility ($\theta = 0.5$, Fig. 3b), and intermediate miscibility ($\theta = 0.7$, Fig. 3c). A binary nematic interaction parameter of $w = -0.32$ was used, for reasons that will be explained later. In the case of low miscibility, shown in Fig. 3a, a broad region of biphasic equilibrium, corresponding to the coexistence between an isotropic and a crystal phase, exists above $T_{NI}$. A homogeneous isotropic phase exists only at very high temperature. Moreover, the LC-rich phase is virtually pure liquid crystal, indicating that all the NPs are phase separated. According to the model, the NP-rich phase should be crystalline, although this was not confirmed experimentally. For a system with high miscibility, as shown in Fig. 3b, the I + C coexistence region is shifted to lower temperatures, and a homogeneous isotropic phase exists for a low concentration of NP above $T_{NI}$, indicating that some amount of NPs is dissolved in the LC-rich phase. For a case of intermediate miscibility, as shown in Fig. 3c, there is some degree of miscibility but the LC-rich phase is very close to the pure LC axis, indicating that only a small amount of NPs can be dissolved in the isotropic phase in the vicinity of $T_{NI}$.

Fig. 4 shows the phase diagrams in the region of very low concentration of NPs, in the vicinity of $T_{NI}$ (which are the relevant experimental conditions). In Fig. 4a, corresponding to the case of high miscibility, it can be seen that a region of homogeneous nematic solutions exists, indicating that the nematic phase can dissolve some amount of NPs. This is due to the use of a negative nematic interaction parameter $w$. This phase behaviour matches qualitatively the experimental observation of the existence of a homogeneous nematic phase for very low concentrations of NPs. In Fig. 4b, corresponding to intermediate miscibility, it can be seen that only a small amount of NPs (approximately 0.003 in volume with this phase diagram) can be dissolved in the isotropic phase close to $T_{NI}$. If the mixture has a higher concentration of NPs, some of them will be dissolved and the remaining NPs will form aggregates (corresponding to the experimental observation of partial solubility).

Now we consider what happens when a mixture is quenched to below $T_{NI}$. When the NPs are completely soluble in the isotropic phase, two different cases can be met, shown by the arrows in Fig. 4a. If the NP concentration is very low (shown by the arrow at a volume fraction of 0.0025), the systems first enter into a narrow I + N coexistence, and as the temperature is further decreased it enters into a region of homogeneous nematic phase, as discussed before. If the temperature range of I + N coexistence is narrow enough, this effect will not be noticeable (no phase separation below $T_{NI}$, as observed experimentally) and the behaviour of this system will be similar to that of a pure LC. If the NP concentration is higher (0.005 volume fraction, corresponding approximately to 1 wt%), the system will be always in a coexistence region (I + N or C + N) below $T_{NI}$. In this case, the system is initially isotropic but as the temperature decreases below $T_{NI}$ the equilibrium amount of the nematic phase grows rapidly to the point where the nematic phase is predominant (as can be seen by applying the lever rule), so nematic droplets are initially nucleated from the isotropic phase, but they rapidly grow and coarsen until they fill most of the space, giving rise to the cellular network structure observed experimentally.

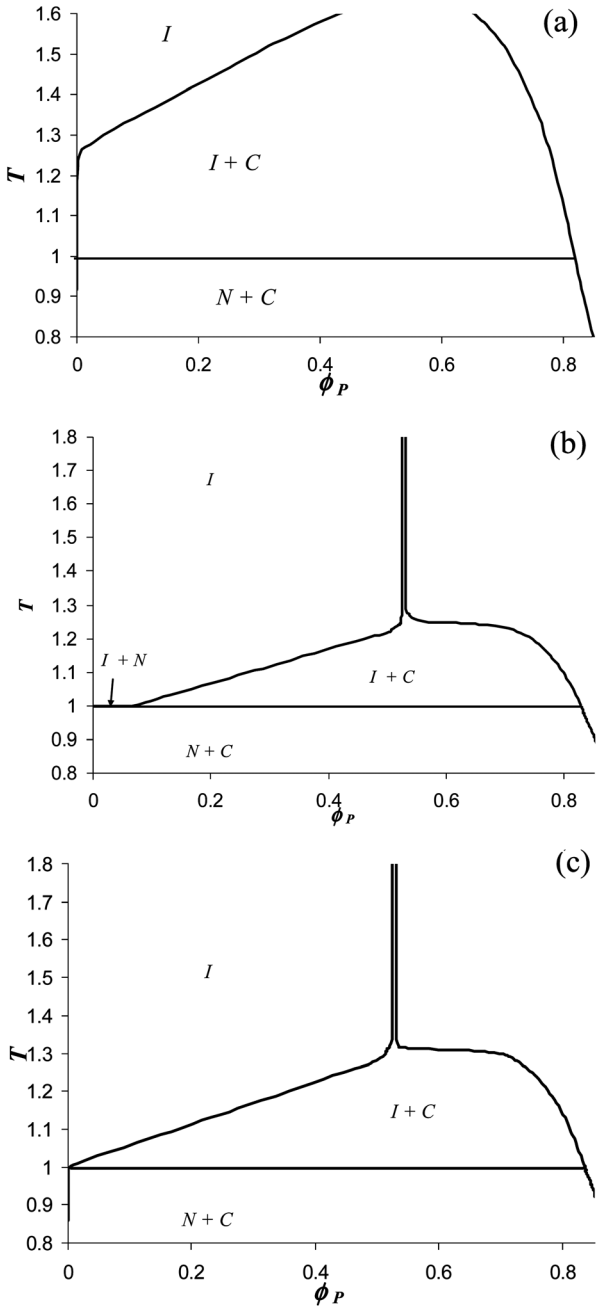


**Fig. 3** Calculated phase diagrams for NPs with different contents of mesogenic ligands: 0% (a), 49% (b), and 70% (c).

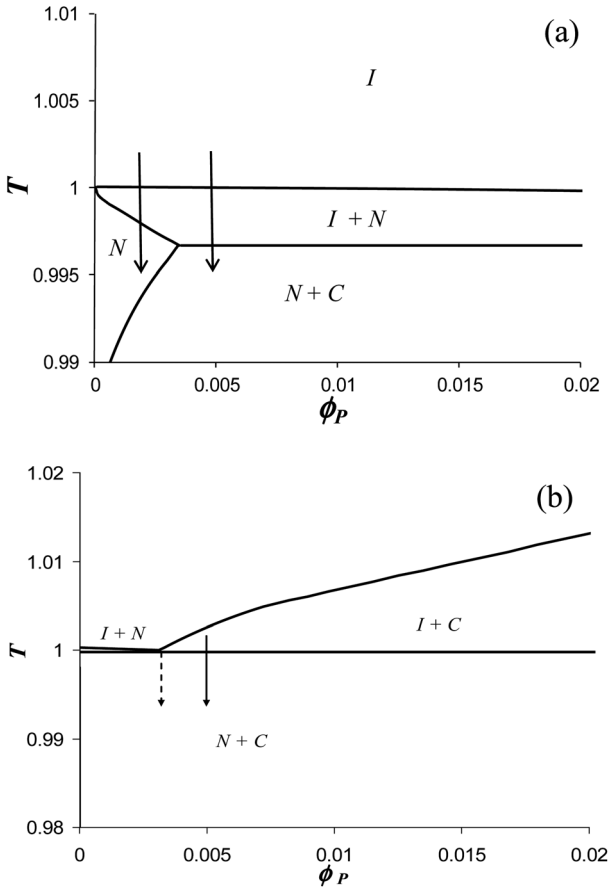


**Fig. 4** Phase diagrams in the low NP concentration region for NP-49 (a) and NP-70 (b). The solid and dashed arrows indicate different trajectories, corresponding to different quenches from the isotropic to the nematic state.

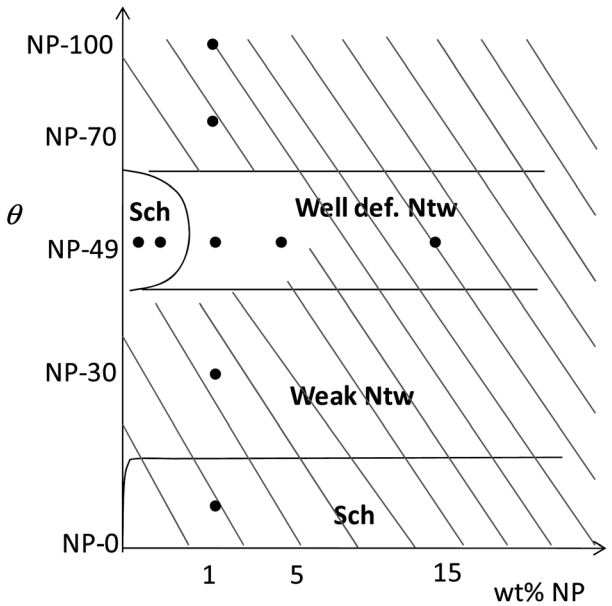


**Fig. 5** Qualitative structure diagram, showing the expected structures as a function of NP type and NP concentration in the dispersion. The plane is divided into three areas corresponding to Schlieren textures (Sch), weak network (Weak Ntw) and well-defined network (Well def. Ntw). The shaded area corresponds to the formation of aggregates. As the plot is qualitative, an exact scale is not given, but the location of the experimental systems studied is indicated by the black dots.

In the case of partial miscibility, illustrated in Fig. 4b, a phase equilibrium exists above $T_{NI}$, and some amount of particles are initially segregated forming aggregates, so the NP concentration in the majority phase is lower than the global NP concentration. As the system is quenched, the system enters into the N + C coexistence region and the isotropic phase is transformed into the nematic and crystalline phase, leading to a cellular network structure. If the aggregates formed initially are stable, they can remain as individual aggregates after this process and the final structure will be equivalent to that of a mixture with a lower initial NP concentration, as shown by the dotted arrow in Fig. 4b (the dotted arrow shows the extreme case where the concentration in the isotropic phase above $T_{NI}$ is the equilibrium concentration).

Several factors will determine the final amount of isotropic phase: higher solubility of NPs in the nematic phase, lower solubility of LC in the crystal phase, and lower initial concentration of the isotropic phase undergoing the I–N transition, favouring a smaller amount of isotropic phase. If mixtures with 0.005 volume fraction are compared, for the high miscibility case some amount of NPs is dissolved in the nematic phase, but the initial concentration of the isotropic phase is lower and the solubility of LC in the crystal phase is lower for the case of partial miscibility, so the final result is that the amount of isotropic phase is lower in the case of partial miscibility (Table 1). If systems of 1 and 15 wt% Au NP-49 are compared, in the later the initial concentration of the isotropic phase is much higher, so a higher amount of isotropic phase is observed.

From all the previous analysis, a rough morphology diagram can be constructed, where the different structures are indicated as a function of the type of NP and its concentration in the mixture. This is shown qualitatively in Fig. 5, where the locations of the experimental systems are indicated. Formation of Schlieren textures, weak networks and well defined networks are indicated, as well as the formation of aggregates.

## 5. Conclusions

A combined experimental and theoretical analysis of phase equilibrium and phase transitions in dispersions of gold nanoparticles capped with mixed ligand monolayers in a calamitic liquid crystal was performed. The effects of NP concentration and ligand monolayer composition on the initial solubility and the final structure were analyzed. A higher solubility was found for a mixed monolayer, while NPs with a pure alkylic shell showed the lowest solubility. High miscibility and high concentrations of NPs favoured the formation of a well defined (in terms of contrast) network structure, while low solubility and very low concentrations on NPs favoured the formation of Schlieren textures. A phenomenological expression for the isotropic interaction parameter, accounting for entropic and enthalpic effects, was proposed to explain the observed solubility trend, and a qualitative explanation of the observed structures was provided in terms of the calculated phase diagrams. It was shown that important aspects of the final structure (cellular network

*versus* Schlieren texture, isotropic phase *versus* defect walls) were determined by the phase equilibrium behaviour.

Most of the previous experimental and theoretical studies of NP dispersions in liquid crystals were restricted to low particle concentrations. High NP concentrations have not been explored experimentally to avoid uncontrolled particle aggregation. The presented integrated theory and experimental study provides a step towards a rational development path to produce and control the structures and morphologies of highly concentrated NP–LC dispersions by first understanding the phase equilibrium behavior. Current studies now focus on the kinetics of the phase separations leading to the formation of long-range, quasi-periodic nanoparticle networks within LC matrices. Mesophase-based nanocomposites are versatile materials with highly promising eletro-optical, functional, sensor/actuator, and biomimetic potential. Prominent examples of current and future work in this area include mixing carbon mesophases with CN for high performance superfibers and biomimetic liquid crystal templating to produce multiscale morphologies found in biological tissues. The potential of mesophase nanoscience will require a fundamental understanding of thermodynamics and structure formation, as presented in this paper.

## Acknowledgements

This work was supported by Le Fonds Quebecois de la Recherche sur la Nature et les Technologies (FQNRT, Quebec). ADR acknowledges partial support by the U.S. Office of Basic Energy Sciences, Department of Energy, grant DE-SC0001412.

## Notes and references

1 A. M. Donald, A. H. Windle and S. Hanna, *Liquid Crystalline Polymers*, Cambridge University Press, Cambridge, 2nd edn, 2006.
2 B. Bahadur, *Liquid Crystals: Applications and Uses*, World Scientific, New Jersey, 1992.
3 C. Paquet and E. Kumacheva, *Mater. Today*, 2008, **11**, 48.
4 P. S. Drzaic, *Liquid Crystal Dispersions*, World Scientific, Singapore, 1995.
5 J. Cleaver and W. C. K. Poon, *J. Phys.: Condens. Matter*, 2004, **16**, S1901.
6 V. J. Anderson, E. M. Terentjev, S. P. Meeker, J. Crain and W. C. K. Poon, *Eur. Phys. J. E: Soft Matter Biol. Phys.*, 2001, **4**, 11.
7 P. G. Petrov and E. M. Terentjev, *Langmuir*, 2001, **17**, 2942.
8 S. P. Meeker, W. C. K. Poon, J. Crain and E. M. Terentjev, *Phys. Rev. E: Stat. Phys., Plasmas, Fluids, Relat. Interdiscip. Top.*, 2000, **61**, R5083.
9 R. Pratibha, W. Park and I. I. Smalyukh, *J. Appl. Phys.*, 2010, **107**, 063511.
10 M. Tasinkevych and D. Andrienko, *Condens. Matter Phys.*, 2010, **13**, 33603.
11 P. Poulin and D. A. Weitz, *Phys. Rev. E: Stat. Phys., Plasmas, Fluids, Relat. Interdiscip. Top.*, 1998, **58**, 626.
12 J. C. Loudet, P. Barois, P. Auroy, P. Keller, H. Richard and P. Poulin, *Langmuir*, 2004, **20**, 11336.
13 P. V. Dolganov, H. T. Nguyen, G. Joly, V. K. Dolganov and P. Cluzeau, *Europhys. Lett.*, 2007, **78**, 66001.
14 R. A. Vaia and J. F. Maguire, Polymer nanocomposites with prescribed morphology: going beyond nanoparticle-filled polymers, *Chem. Mater.*, 2007, **19**, 2736.
15 A. C. Balazs, T. Emrick and T. P. Russell, *Science*, 2006, **314**, 1107.
16 R. Krishnamoorti, *MRS Bull.*, 2007, **32**, 341.
17 J. W. Goodby, I. M. Saez, S. J. Cowling, V. Gartz, M. Draper, A. W. Hall, S. Sia, G. Cosquer, S. E. Lee and E. P. Raynes, *Angew. Chem., Int. Ed.*, 2008, **47**, 2754.
18 M. R. Bockstaller, Y. Lapetnikov, S. Margel and E. L. Thomas, *J. Am. Chem. Soc.*, 2003, **125**, 5276.
19 A. Matsuyama and R. Hirashima, *J. Chem. Phys.*, 2008, **128**, 044907.
20 E. R. Soulé, L. Reven and A. D. Rey, *Mol. Cryst. Liq. Cryst.*, 2012, **552**, 118–126.
21 J. Milette, V. Toader, L. Reven and R. B. Lennox, *J. Mater. Chem.*, 2001, **21**, 9043.
22 V. V. Ginzburg, *Macromolecules*, 2005, **38**, 2362.
23 E. R. Soulé, J. Borrajo and R. J. J. Williams, *Macromolecules*, 2007, **40**, 8082.
24 E. R. Soulé, C. E. Hoppe, J. Borrajo and R. J. J. Williams, *Ind. Eng. Chem. Res.*, 2010, **49**, 7008.
25 W. Maier and A. Saupe, *Z. Naturforsch., A: Phys., Phys. Chem., Kosmophys.*, 1959, **14**, 882.
26 W. Maier and A. Saupe, *Z. Naturforsch., A: Phys., Phys. Chem., Kosmophys.*, 1960, **15**, 287.
27 E. R. Soulé and A. D. Rey, *Liq. Cryst.*, 2011, **38**, 201.
28 J. Milette, V. Toader, C. Lavigne, R. B. Lennox, L. Reven, S. Cowling, I. M. Saez and J. W. Goodby, *Soft Matter*, 2012, **8**, 173–179.
29 H. Qi and T. Hegmann, *ACS Appl. Mater. Interfaces*, 2009, **1**, 1731.
30 H. Qi, B. Kinkead, V. M. Marx, H. R. Zhang and T. Hegmann, *ChemPhysChem*, 2009, **10**, 1211.



 